CHEMISTRY OF MATERIALS
Article

Chem. Mater. **2011,** *23,* 907–912 907
DOI:10.1021/cm102463t

Molecular-Scale and Nanoscale Morphology of P3HT:PCBM Bulk Heterojunctions: Energy-Filtered TEM and Low-Dose HREM†

Lawrence F. Drummy,*,‡ Robert J. Davis,§ Diana L. Moore,§ Michael Durstock,‡ Richard A. Vaia,‡ and Julia W. P. Hsu⊥

‡*Materials and Manufacturing Directorate, Air Force Research Laboratory, WPAFB, Ohio 45433, United States,* §*Sandia National Laboratory, Albuquerque, New Mexico 87815, United States, and* ⊥*Center for Integrated Nanotechnologies, Sandia National Laboratories, Albuquerque, New Mexico 87185, United States*

Received August 27, 2010. Revised Manuscript Received November 5, 2010

The performance of bulk heterojunction organic photovoltaic devices is critically dependent on the morphology of the active layer. Here we describe the combination of two electron microscopy techniques to quantitatively examine the molecular level structure and mesoscopic domain morphology of the active layer of poly(3-hexylthiophene):[6,6]-phenyl-C_{61}-butyric acid methyl ester P3HT:PCBM bulk heterojunction solar cells. Energy-filtered transmission electron microscopy (EFTEM) revealed the nanoscopic, interpenetrating fibrillar structure of the phase separated blend, providing unique assignments of the P3HT-rich and PCBM-rich regions. Low-dose high-resolution electron microscopy (LD-HREM) provided direct images of the P3HT crystals and their orientation within the P3HT-rich domains. The high mobility [010] crystallographic direction of these crystals coincides with the P3HT fibril axis. Additionally, the width of the P3HT crystallite coincides with the width of the P3HT-rich fibril, and is less than that of P3HT crystals in comparably processed pure P3HT films. The local crystallite structure within the blend is commensurate with the constraints of the nanoscale interpenetrating morphology and confirms the intimate relationship between processing protocols, which define the mesoscale phase-separated domains, and the molecular level ordering within the domains, which determines local transport characteristics.

Introduction

Organic photovoltaics have shown potential for replacing silicon-based photovoltaics in select applications, because of their low cost and versatile processing. Significant materials challenges remain before the efficiencies of current devices are high enough to make organic photovoltaics a viable technology.[1−3] One key challenge is that because of the relatively high exciton binding energy in organic materials as compared to silicon, excitons do not dissociate freely, rather they must first diffuse to a donor−acceptor interface before being separated. Quantitative information pertaining to the size-scale of the donor and acceptor phases, and the morphology of the donor−acceptor interface, is therefore critical for understanding structure−property relationships in organic photovoltaics. Additionally, because the carrier mobilities of organics are highly dependent on the local degree of structural ordering, and high mobilities are needed to move charges to their respective electrodes for current generation in a solar cell, it is critical to characterize local order at the molecular level within each of the donor and acceptor phases.

Because a balance between exciton diffusion to the interfaces for charge separation and transport of the resulting electron and holes in their respective phases to the electrodes is believed to be critical for achieving high efficiency solar cells, the length scale of phase separation should be matched to the exciton diffusion length, which has been characterized for conducting polymers to be 3−15 nm.[4−7] Current efforts toward this goal have been largely empirical with device performance as feedback, as the morphology of P3HT:PCBM bulk heterojunctions[8−10] is difficult to uniquely discern because of the nanoscale phase separation and the low overall degree of ordering. Nevertheless, there are a few features that have consistently been characterized via transmission electron microscopy (TEM) techniques, and that have been shown to impact device performance in a reproducible manner. The first is that the length scale of the phase

† Accepted as part of the "Special Issue on π-Functional Materials".

*Corresponding author. E-mail: lawrence.drummy@wpafb.af.mil.

(1) Coakley, K. M.; McGehee, M. D. *Chem. Mater.* **2004**, *16*, 4533–4542.
(2) van Bavel, S. S.; Loos, J. *Adv. Funct. Mater.* **2010**, *20*, 3217–3234.
(3) Groves, C.; Reid, O. G.; Ginger, D. S. *Acc. Chem. Res.* **2010**, *43*, 612–620.
(4) Haugeneder, A.; et al. *J. Phys. Rev. B* **1999**, *59*, 15346.
(5) Theander, M.; et al. *Phys. Rev. B* **2000**, *61*, 12957.
(6) Kroeze, J. E.; Savenije, T. J.; Vermeulen, M. J. W.; Warman, J. M. *J. Phys. Chem. B* **2003**, *107*, 7696.
(7) Liang, Z.; Nardes, A.; Wang, D.; Berry, J. J.; Gregg, B. A. *Chem. Mater.* **2009**, *21*, 4914–4919.
(8) Van Bavel, S. S.; Sourty, E.; de With, G.; Loos, J. *Nano Lett.* **2009**, *9*, 507–513.
(9) Savenije, T. J.; Kroeze, J. E.; Yang, X.; Loos, J. *Adv. Funct. Mater.* **2005**, *15*, 1260–1266.
(10) Li, L.; Lu, G.; Yang, X. *J. Mater. Chem.* **2008**, *18*, 1984–1990.

Published on Web 11/30/2010

separation is dependent on processing conditions, but typically on the order of 10 nm.[8−10] The second is that anisotropic structures, attributed to P3HT fibrils, have been visualized in the blends, and the aspect ratios of these features are tailorable by varying processing conditions. Examples of such process variables include precrystallization of P3HT and subsequent blending in PCBM,[10] or postfilm formation thermal anneal,[9] or solvent-assisted anneal.[8] However, the local molecular-scale organization within each phase and its relationship to the domain structure has not been characterized. This work demonstrates a combination of experimental techniques that address this uncertainty so as to provide methods to examine the processing-structure-efficiency relationship and answer fundamental questions such as how does nanoscale morphology impact molecular scale organization.

For nanostructured blends such as P3HT:PCBM, the local concentration of each constituent is unknown and the densities may deviate from bulk due to confinement effects. Thus even though the densities of the pure materials can be measured independently in standard bright-field TEM images of uniform films, assignment of bright-field scattering contrast to the imaged phases in P3HT:PCBM blends is difficult. Furthermore, local densities and contrast in semicrystalline organic materials change with electron beam exposure because of beam damage (electron-induced crystalline to amorphous transition[12,13] and/or mass loss[14,15]). We show that these challenges can be addressed by combining energy-filtered transmission electron microscopy (EFTEM) and low-dose high-resolution electron microscopy (LD-HREM). EFTEM[16−19] provides image contrast based on the local material electronic signature through the electron energy loss spectrum, and does not rely solely on assumptions about local material density, as are necessary to interpret bright-field TEM images.[20,21] In LD-HREM lattice images of crystals can be obtained if the total irradiation dose at the sample is kept well below the critical dose for damage of crystallinity.[22] We show that when combined, these two techniques provide a wealth of nanoscale and molecular-level morphology information critical for building structure−property relationships in organic photovoltaic materials.

Experimental Section

P3HT, PCBM, and P3HT:PCBM blend films for EELS and HREM analysis were deposited on Si substrates coated with a layer of PEDOT:PSS (Clevios P VP 4083). The Si substrates were sonicated in soapy water and isopropyl alcohol for 10 min each, followed a 15 min UV ozone treatment. The PEDOT:PSS layer was spun on the clean Si at 2000 rpm for 1 min and dried on a hot plate at 120 °C for 10 min. P3HT films were prepared using a solution of 15 or 30 g/L P3HT (Rieke Metals, electronics grade regioregular P3HT 4002-E) in *o*-dichlorobenzene (Acros Organics, 99+%), dissolved while heating at 60 °C for 30 min and then spun at 1000 rpm for 1 min to produce 50 and 100 nm thick polymer films respectively. The P3HT films were dried in the dark in N_2 overnight and subsequently annealed on a hot plate at 110 °C for 10 min in N_2. The 10 nm thick P3HT film was spun onto Si/PEDOT from 1.3 g/L P3HT dissolved in chlorobenzene (Sigma Aldrich, 99.8%) while heating at 60 °C for 30 min, and was then annealed on a hot plate at 110 °C for 10 min in N_2. PCBM films were spun onto Si/PEDOT substrates from a solution of 18 g/L PCBM (Nano C, C_{60}PCBM >99.5%) in chlorobenzene, dissolved while heating at 80 °C for 30 min and then spun at 1000 rpm for 1 min. P3HT:PCBM films were spun onto Si/PEDOT substrates from a solution of 2.6 g/L, 30 g/L or 60 g/L P3HT:PCBM in a 1:1 weight ratio in *o*-dichlorobenzene, dissolved while heating at 60 °C for 30 min and spun at 600 rpm for 1 min, producing 20, 100, and 200 nm thick films, respectively. After drying overnight in the dark in a N_2 atmosphere, the P3HT:PCBM films were annealed on a hot plate at 110 °C for 10 min in N_2.

For transmission electron microscopy, films were floated off the substrates onto deionized water, dissolving the PEDOT:PSS layer, and films were collected onto 400 M Cu grids. Microscopy was performed on a C_s-corrected FEI Titan operating at 300 kV with low-dose system and a GIF Tridiem. Conditions for low dose HREM in the image acquisition mode were: spot size 10, 27 kX magnification, 1 s exposure time, screen current 1 pA/cm^2, total dose received by sample of ~.001 C/cm^2. Focusing was performed on an adjacent area 1 μm away from the imaged area. An optimum defocus condition for the 1.6 nm (100) spacing was an underfocus of 650 nm. EFTEM images were collected on a GIF Tridiem on an FEI Titan at 300 kV. Zero loss peak was aligned on the CCD in spectroscopy mode and then in imaging mode. The full width at half maximum intensity of the zero loss peak after alignment was 1.0 eV. The spectrum was shifted to the desired energy for EFTEM imaging. Collection aperture was 2 mm, and the slit width was 8 eV for EFTEM imaging.

The processing conditions used to make the P3HT:PCBM active layer used in the TEM experiment produce inverted bulk heterojunction solar cells (ITO/ZnO/P3HT:PCBM/PEDOT/Ag) with power conversion efficiency of 2.4% (V_{oc} of 600 mV, J_{sc} of 7.8 mA/cm^2, and fill factor of 52%; see Figure S1 in the Supporting Information), comparable to previously published device results.[23] Patterned ITO substrates (Thin Film Devices, Anaheim CA) were sonicated in soapy water and isopropyl alcohol for 10 min each, followed by a 15 min UV ozone treatment. A zinc acetate solution 7.7 g/L in ethanol was spin-coated at 1000 rpm onto the ITO and pyrolyzed in air on a hot plate at 150 °C for 10 min. The spin-coating/pyrolysis was repeated once to form a 15 nm total thickness ZnO film.[24] A 60 g/L solution of P3HT:PCBM in a 1:1 weight ratio was used to fabricate the active layer following the spinning, drying, and annealing procedures described in the previous paragraph. Organic and ZnO layer thicknesses were confirmed by UV−vis spectroscopy (Ocean Optics, Inc.). A PEDOT:PSS layer was then spun at 2000 rpm for 1 min onto the active layer from a PEDOT solution with 1% by weight surfactant

(11) Yang, X.; et al. *Nano Lett*. **2005**, *5*, 579–583.
(12) Kumar, S.; Adams, W. W. *Polymer* **1990**, *31*, 15–19.
(13) Drummy, L. F.; Yang, J.; Martin, D. C. *Ultramicroscopy* **2004**, *99*, 247.
(14) Varlot, K.; Martin, J. M.; Quet, C. *Micron* **2001**, *32*, 371.
(15) Bermudez, V. M. *J. Vac. Sci. Technol., B* **1999**, *17*, 2512.
(16) Siangchaew, K.; Libera, M. *Microsc. Microanal*. **1997**, *3*, 530–539.
(17) Lieser, G.; Schmid, S. C.; Wegner, G. *J. Microsc*. **1996**, *183*, 53–59.
(18) DuChesne, A. *Macromol. Chem. Phys*. **1999**, *200*, 1813–1830.
(19) Daniels, H. R.; Brydson, R.; Brown, A.; Rand, B. *Ultramicroscopy* **2003**, *96*, 547–558.
(20) Reimer, L. *Transmission Electron Microscopy: Physics of Image Formation and Microanalysis*, 4th ed.; Springer: Berlin, 1997.
(21) Spence, J. C. H. *High Resolution Electron Microscopy*, 3rd ed.; Oxford University Press: Oxford, U.K., 2003.
(22) Martin, D. C.; Thomas, E. L. *Polymer* **1995**, *36*, 1743–1759.
(23) White, M.; Olson, D.; Shaheen, S.; Kopidakis, N.; Ginley, D. *Appl. Phys. Lett*. **2006**, *89*, 143517.
(24) Lee, Y.-J et al. IEEE J. Sel. Top. Quantum Electron. **2010**, in press.

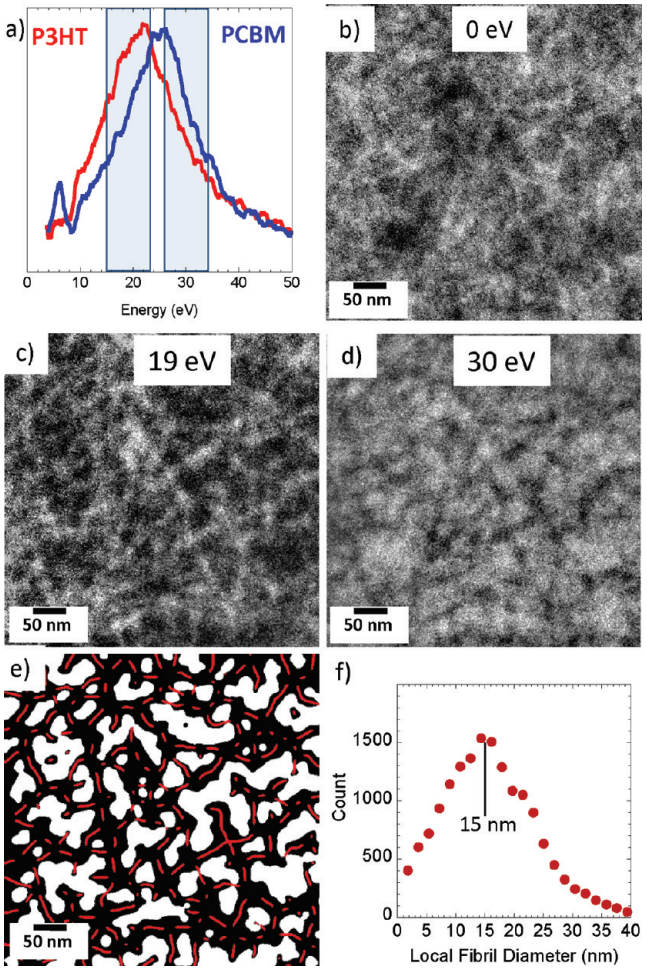

Figure 1. Energy-filtered transmission electron microscopy of a 100 nm thick 50:50 (w/w) blend of P3HT and PCBM. (a) EELS spectra from pure P3HT and pure PCBM films. Energy windows are drawn at 19 ± 4 eVand 30 ± 4 eV, where inelastic scattering is more intense from P3HT and PCBM, repectively. (b) Zero loss image formed using only elastically scattered electrons. (c) 19 eV loss image, where P3HT domains are bright. (d) 30 eV image, where PCBM domains are bright. (e) Segmented image from c with skeleton of fibrils overlaid in red. (f) Distribution of local fibril diameters (15 ± 8 nm) calculated from the skeleton of the Euclidian distance map.

added (Aldrich, Zonyl 100) to aid wetting on the polymer film. The PEDOT film was dried on a hot plate at 120 °C for 10 min in air. Silver electrodes 100 nm thick were thermally evaporated over the P3HT through a shadow mask to define a device area of 0.1 cm^2. Device measurements under simulated one-sun condition were carried out with a KG5 filtered tungsten-halogen lamp with an intensity of 100 mW/cm^2 as determined by a NREL calibrated Si photodiode.

Results and Discussion

Elecron energy loss spectroscopy (EELS) results from neat P3HT and PCBM films are shown in Figure 1a. Noteworthy features in the spectra include the 6 eV $\pi-\pi^*$ electronic transition in PCBM, as well as broader peaks between ~10 and ~40 eV in both materials arising from collective oscillations of valence electrons.[25] The $\pi-\pi^*$ in P3HT occurs at 2.3 eV,[26] which is energetically too low to be detected in our microscope, and the 6 eV PCBM peak, although resolved in the EELS spectrum, was too close to the zero-loss peak for imaging with adequate slit widths (8 eV slit width used here). In this study, we use 19 eV to image P3HT and 30 eV to image PCBM. Because differences in the electronic structure of each material are reflected in the higher energy regions of the EELS spectrum (~10−40 eV), this provided complementary contrast for each phase in the structured blends. Figure 1b shows the zero-loss image, formed with only elastically scattered electrons. This is similar to a typical bright-field image, where the contrast is primarily due to local density differences, which have been reported for pure P3HT[27] (1.1 g/cm^3) and pure PCBM[28] (1.5 g/cm^3). EFTEM thickness maps (Figure S5 in the Supporting Information) show smooth films, with no contrast fluctuations at length scales comparable to the features visible in Figure 1c,d. A fibular network morphology is visible in the zero loss image, consistent with other bright-field TEM reports.[9,11] In contrast to the zero-loss image, Figure 1c shows the EFTEM image of the same region where the energy window is centered at 19 ± 4 eV, corresponding to enhanced EELS intensity from P3HT. Therefore the bright regions in the image correspond to the P3HT-rich domains. Figure 1d shows the same region of sample at 30 ± 4 eV in which the PCBM-rich domains appear bright. The image intensity here is effectively inverted from the 19 ± 4 eV image. Together, these EFTEM images provide an unambiguous assignment of the phases, rather than the notional assignments in bright field. Qualitatively, the P3HT-rich domains create a well-connected network, as isolated P3HT fibrils are rarely visible. Similar morphologies were observed for P3HT:PCBM films of other thicknesses, although the network structure appeared less developed for the thinner films, and overlap of projection regions obscured crisp interfaces in the thicker films (see the Supporting Information). Note that for all images in Figure 1, a small objective lens defocus of 2±1 μm was used to minimize phase contrast artifacts from the amorphous components of the materials.[21] Although it is not possible to quantify three-dimensional morphological features from two-dimensional projection images, certain features, such as fibril diameter, can be quantified from 2D projections.[29]

The Euclidian distance map (EDM) of the segmented 19 ± 4 eV image (Figure 1e) was used to calculate the local fibril diameter distribution (Figure 1f), which shows a peak at 15 nm ±8 nm. This is consistent with the 14 nm dominant structural feature size revealed in the digital fast Fourier transform (FFT) analysis of the same image. The size of the PCBM-rich regions in the segmented image, as characterized by the radius of the largest inscribed circle, is 10.6 nm ±4.3 nm (see supplemental).

(25) Barbarez, M. K.; Das Gupta, D. K.; Hayward, D. *J. Phys. D.: Appl. Phys.* **1977**, *10*, 1789–1800.
(26) Ahn, H.; Oblas, D. W.; Whitten, J. E. *Macromolecules* **2004**, *37*, 3381–3387.
(27) Prosa, T. J.; Winokur, M. J.; Moulton, J.; Smith, P.; Heeger, A. J. *Macromolecules* **1992**, *25*, 4364–4372.
(28) Bulle-Lieuwma, C. W. T.; et al. *Appl. Surf. Sci.* **2003**, *203−204*, 547–550.
(29) Russ, J. C. *The Image Processing Handbook*, 5th ed.; Taylor & Francis: Boca Raton, FL, 2007.

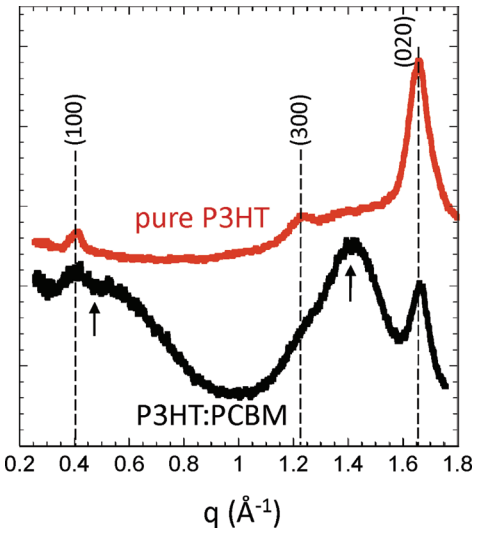

Figure 2. Low-dose energy filtered (zero-loss) electron diffraction of a pure P3HT film (red) and P3HT:PCBM film (black), which displays peaks from both phases. Peaks from the P3HT crystals are shown with dashed lines, and all indices refer to the monoclinic P3HT crystal structure of Brinkmann et al. Arrows show the broad peaks from the PCBM phase.

With a quantitative understanding of the nanophase distribution of P3HT and PCBM, LD-HREM provides insight to the local molecular level organization within the domains. Energy-filtered (zero-loss) electron diffraction of the P3HT:PCBM film (Figure 2, black curve) shows two broad peaks from the PCBM phase centered at approximately $q = 2\pi/d = 0.5$ Å^{-1} ($d = 1.3$ nm) and $q = 1.4$ Å^{-1} ($d = 0.45$ nm), as well as three narrow reflections from crystalline P3HT, corresponding to the (100), (300), and (020) planes. Also visible in the pure P3HT (red curve) is a broad hump from amorphous P3HT centered near 1.5 Å^{-1}. The fraction of crystallinity in pure high molecular weight P3HT depends on processing conditions and has been determined to be in the range of 4−18%.[30,31] These features are observed in the energy filtered electron diffraction from films of the pure constituents. The critical electron dose for destruction of crystallinity in P3HT was determined to be 0.010 ± 0.002 C/cm^2 at 300 kV by monitoring the fading of the P3HT (020) reflection. This is similar to prior reports of semiconducting polymers, such as poly(nonylbithiazole) (0.018 C/cm^2).[32] The intensity and width of the broad PCBM peaks did not change with this electron irradiation. Thus, to ensure sample stability for LD-HREM, the maximum electron dose used was 0.001 C/cm^2.

For PCBM, the reflections are broader than expected if local order was crystalline and peak broadening arose from finite crystal size (i.e., nanocrystallites).[33] Scherrer analysis of peak breadth of the $q = 0.5$ Å^{-1} peak implies coherent lattice order of 1.7 nm, which is on the order of 2 PCBM molecules. Hence, the breadth of these reflection indicates that the PCBM is paracrystalline or amorphous.

Consistent with the electron diffraction, only amorphous structure was visualized in the pure PCBM and PCBM-rich domains of the blended films using LD-HREM. For P3HT, (100) lattice fringes are observed in both the P3HT:PCBM blend and pure P3HT films (Figure 3a,b), consistent with the presence of (100) crystalline reflections in the electron diffraction. Two possible crystallographic orientations in which the (100) planes are visible, the [010] and [001], are shown in Figure 3c. As shown in the schematic, the (100) planes contain the P3HT crystal *b*-axis and *c*-axis. Furthermore, superposition of LD-HREM and EFTEM images taken sequentially from the same region of sample demonstrates that majority of the P3HT crystals lay within the connected P3HT-rich domains. As an example, the red lines superposed in Figure 3a represent the phase boundary as determined by the segmented 19 eV EFTEM image. The majority of lattice fringes lie within the connected P3HT-rich phase, with the (100) planes parallel to the fibril axis in most instances. Regions in the connected phase where no (100) planes are visible reflect P3HT crystals out of Bragg condition or amorphous P3HT. The few lattice fringes outside these regions probably reflect the projection of ~10 nm features through a 100 nm film thickness. Qualitatively, the crystals in the pure P3HT (Figure 3b) are typically larger in lateral extent perpendicular to the (100) planes than the crystals in the P3HT:PCBM blends. Previous imaging of P3HT crystals in pure P3HT films ($M_N = 5700-34\,000$ g/mol) showed lamellar crystals with the crystal width perpendicular to (100) greater than the length parallel to (100).[34] This is consistent with our observation and shows P3HT forms an altered crystal shape when in nanostructured blends with PCBM.

Figure 4 summarizes the quantitative measurements of the projected size of the P3HT crystallites based on the (100) planes resolved in the LD-HREM micrographs. Crystal length is measured parallel to the (100) planes, crystal width is perpendicular to the (100) planes, and any bending, twist or grain boundaries sufficient to remove the (100) fringes from Bragg condition are considered to be the termination of the crystal. Data were acquired from multiple images similar to images a and b in Figure 3 and compiled for Figure 4. The P3HT crystallites in the P3HT:PCBM blend exhibit a mean size parallel to (100) of 44 ± 28 nm and mean size perpendicular to (100) of 18 ± 4.4 nm, relative to a mean size parallel to (100) of 23 ± 15 nm and a mean size perpendicular to (100) of 26 ± 7.6 nm in pure P3HT films. The projected aspect ratio of the P3HT crystallites in the blend and pure films is 2.5 and 0.88, respectively. A distribution of crystallite orientation with respect to the viewing direction, rather than a change in the crystallite shape, could also account for the observed differences in projected aspect ratio, because the 1.6 nm (100) planes are visible in both the [010] and [001] zone axes, as well as any [0*kl*] zone. Dark-field TEM experiments (see Figure S9 in the Supporting Information) reveal that, on average, the (020) planes are

(30) Zen, A.; et al. *Macromolecules* **2006**, *39*, 2162–2171.
(31) Malik, S.; Nandi, A. K. *J. Polym. Sci., B: Polym. Phys.* **2002**, *40*, 2073–2085.
(32) González-Ronda, L.; Martin, D. C. *Macromolecules* **2004**, *37*, 2872–2879.
(33) Yang, X.; et al. *Adv. Mater.* **2004**, *16*, 802–806.
(34) Brinkmann, M.; Rannou, P. *Macromolecules* **2009**, *42*, 1125–1130.

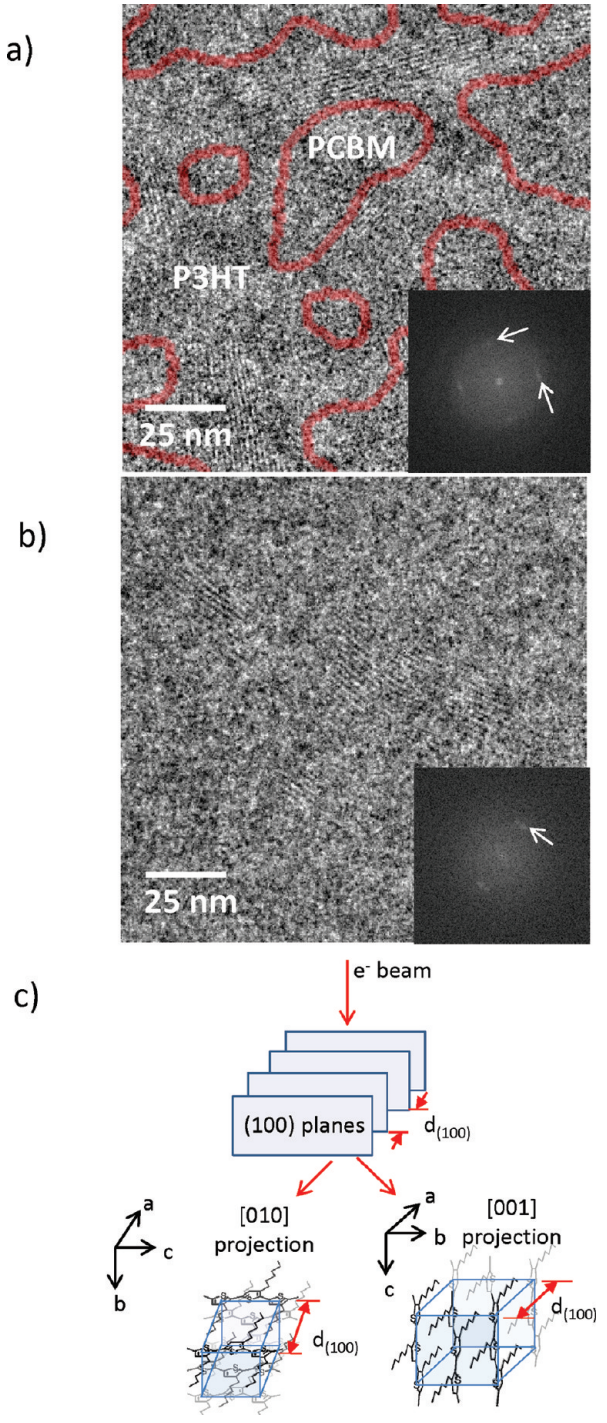

Figure 3. Low-dose high-resolution electron microscopy of P3HT crystal 1.6 nm (100) lattice planes. (a) Combination of the HREM image of 100 nm thick P3HT:PCBM (grayscale image), showing the (100) fringes of the extended P3HT crystals, and the P3HT:PCBM phase boundary as determined by EFTEM (red lines). The P3HT-rich phase is the connected phase bound by the red lines in this image. The P3HT crystals as visualized by HREM lie primarily within the P3HT-rich domains as determined by EFTEM. (b) HREM image from 100 nm thick pure P3HT showing the (100) fringes of the lamellar crystals, which have a wider lateral extent perpendicular to the (100) planes as compared to the P3HT crystals in image a. FFTs inset in a and b show peaks from the 1.6 nm P3HT (100) lattice fringes (shown with arrows). (c) Schematic of the P3HT thiophene-containing (100) planes, previously characterized to be the high-mobility planes in P3HT, and their relation to the unit cell. Regions where the (100) lattice fringes are visible in HREM images are in a [0,*k*,*l*] orientation, with the (100) planes parallel to the electron beam viewing direction. Schematics of two low-index [0,*k*,*l*] projections, the [010] and [001], are depicted here, with the unit cell outlined in blue and the (100) planes shaded in blue.

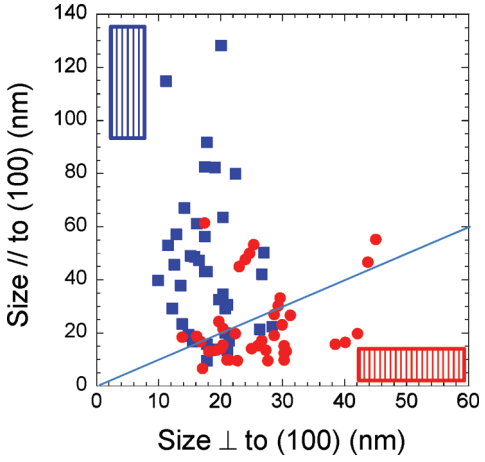

Figure 4. Size distribution of P3HT crystals in pure P3HT 100 nm thick films (red) and P3HT:PCBM 100 nm thick films (blue), as determined by the longitudinal and lateral extent of the (100) lattice fringes in HREM images of P3HT crystals. A line for the aspect ratio of 1 is shown as a guide.

perpendicular to the P3HT fibril axis in the blends. This is consistent with dark-field TEM from pure P3HT whisker films, which also showed (020) perpendicular to P3HT fibrils.[35] In both pure P3HT and P3HT:PCBM, where the (100) are in the Bragg condition and visible in LD-HREM images, the most likely crystal projection is therefore the [001]. Combined with our LD-HREM crystal aspect ratio results in Figure 4, this suggests that for P3HT crystals with (100) in the Bragg condition, there is a difference in P3HT crystal aspect ratio in pure P3HT and 50:50 P3HT:PCBM films processed under the same conditions. P3HT crystals in P3HT:PCBM are anisotropic (aspect ratio 2.5), whereas P3HT crystals in pure P3HT are more isotropic (aspect ratio 0.88).

Combining the crystallite orientation and phase boundaries therefore reveal that on average, the $\pi-\pi$ stacking direction (*b*-axis, [010] direction) in the resolved crystallites align parallel to long axis of the crystallites, which in turn is parallel to the axis of the P3HT fibrils in the blends, schematically shown in Figure 5. As seen in the LD-HRTEM combined with the EFTEM images, the width of the P3HT crystals spans the width of the P3HT fibril. The 18 nm mean crystallite width is similar to the 15 nm diameter of the P3HT fibril width calculated from the segmented EFTEM image (Figure 2b). Furthermore, since the P3HT crystal size parallel to (100) (mean 44 nm) is much larger than the 15 nm fibril diameter, preferred orientation of the crystallite long-axis along the fibril axis results. The polymer chains ([001] direction) are thus on average perpendicular to the domain interface. Additionally, the nominal alkyl chain orientation (*a*-axis, [100]), which coincides with the P3HT low mobility direction,[36−38] is perpendicular to the long axis of the crystals, as well as to the P3HT fibrils. Due to the cylindrical symmetry of the fibrils,

(35) Ihn, K. J.; Moulton, J.; Smith, P. *J. Polym. Sci,. B: Polym. Phys.* **1993**, *31*, 735–742.
(36) Kline, R. J.; McGehee, M. D.; Toney, M. F. *Nat. Mater.* **2006**, *5*, 222–228.
(37) Sirringhaus, H.; et al. *Nature* **1999**, *401*, 685–688.
(38) Chang, J. F.; et al. *Chem. Mater.* **2004**, *16*, 4772–4776.

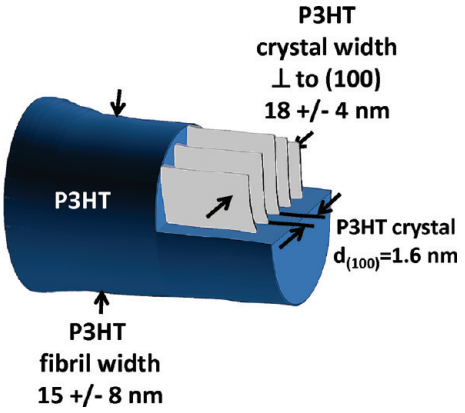

Figure 5. Schematic of the quantitative morphology results from EFTEM and LD-HREM.

(100) planes could be rotated out of the Bragg condition, but still parallel to the fibril axis, in many areas (Figure 5). Because of beam damage constraints, it is not currently possible to take several LD-HREM images of the same fibril at varying tilt angles to resolve these details.

Conclusions

In conclusion, we have made several new observations relating the local molecular level ordering of P3HT and PCBM to the nanoscopic network morphology in the blends. The PCBM phase lacks translational order, and from a device perspective, it is generally accepted that the molecular level ordering of the PCBM is not the limiting factor for carrier mobility in bulk heterojunctions, and that a paracrystalline or amorphous structure, as shown here, is sufficient for device performance.[32] The P3HT crystallite width roughly corresponds with the width of the P3HT fibrils in the EFTEM images, implying that blending with PCBM results in an anisotropic fibril morphology in P3HT crystals, as compared to more isotropic shaped crystals found in similarly processed pure P3HT. Additionally, the (100) lattice planes are nominally straight throughout the crystals, and do not exhibit significant bending as has been observed in other thiophene-related conducting polymers[33] and oligomers.[39] This is likely related to the constraints of the fibril morphology inside of which the crystallites are formed. The P3HT crystals are anisotropic, with the P3HT (100) planes running parallel to the fibril directions, and the [100] direction running perpendicular to the fibril direction. As the (100) planes are the P3HT high-mobility lamellae characterized by Kline et al.,[36] our finding of P3HT crystal orientation in the fibril implies rapid charge removal from the solar cell active layer. Although the $\pi-\pi$ stacking direction is along the fiber axis, the semicrystalline nature implies that transport will be limited by grain boundaries or crystalline–amorphous boundaries within the fibrils. The P3HT fibrils (radius = 7.5 nm) and the PCBM domains (radius = 10.6 nm) are on the order of the exciton diffusion length,[4–7] which is critical for maximizing the efficiency of the charge separation process in this bulk heterojunction system. The combination of EFTEM and LD-HREM is expected to provide similar quantitative morphology details for other ordered organic blend materials to those shown here for bulk heterojunctions.

Acknowledgment. The authors thank Dr. John Russ for helpful discussion regarding image segmentation and quantitative analysis. Microscopy was performed in the Materials Characterization Facility at the Materials and Manufacturing Directorate. The authors acknowledge the Air Force Office of Scientific Research, the Air Force Research Laboratory and the Materials and Manufacturing Directorate for funding. This work was performed, in part, at the Center for Integrated Nanotechnologies, a U.S. Department of Energy, Office of Basic Energy Sciences user facility. Sandia is a multiprogram laboratory operated by Sandia Corporation, a Lockheed Martin Company, for the United States Department of Energy under contrast DE-AC04-94AL85000.

Supporting Information Available: Additional information and figures (PDF). This material is available free of charge via the Internet at http://pubs.acs.org.

(39) Lovinger, A. J.; Katz, H. E.; Dodabalapur, A. *Chem. Mater.* **1998**, *10*, 3275–3277.